Journal of Materials Chemistry A

Accepted Manuscript

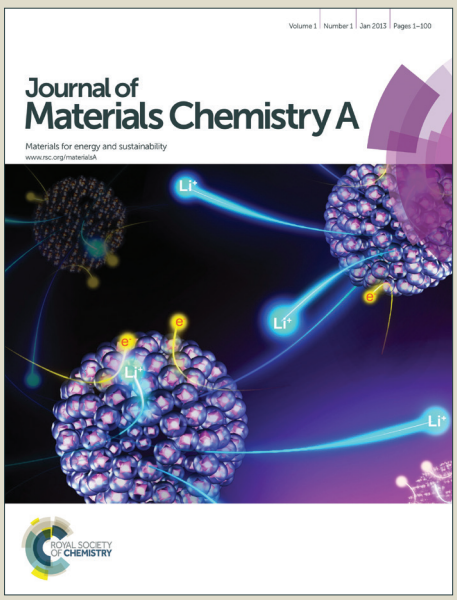

ROYAL SOCIETY OF CHEMISTRY

www.rsc.org/materialsA

Rationally Designed Hierarchical $ZnCo_2O_4/Ni(OH)_2$ Nanostructures for High-Performance Pseudocapacitor Electrodes

H. X. Chuo,[a] H. Gao, [a] Q. Yang, [a] N. Zhang, [b] W. B. Bu [a] and X. T. Zhang [*,a]

[a] *Key Laboratory for Photonic and Electronic Bandgap Materials, Ministry of Education，School of Physics and Electronic Engineering, Harbin Normal University, Harbin 150025, P. R. China.*

[b] *Department of Chemistry and Chemical Biology, Cornell University, Ithaca, USA.*

Abstract:

Hierarchical $ZnCo_2O_4/Ni(OH)_2$ nanostructures on Ni foam were rationally designed and successfully fabricated through a facile two-step growth method. The $ZnCo_2O_4$ nanowires grown on Ni foam were served as backbones to improve the electrical conductivity of redox active $Ni(OH)_2$ electrode materials, enhance the surface areas of electrode materials, and solidify the $Ni(OH)_2$ electrode materials onto Ni foam as current collector. $Ni(OH)_2$ nanosheets were electrodeposited on the $ZnCo_2O_4$ nanowires. The electrochemical performances of the hierarchical $ZnCo_2O_4/Ni(OH)_2$ nanostructures were measured. Their specific capacitance is 2826 F/g at a current density of 2 mA/cm^2, the good rate capability is 71.4% when the current density increases from 2 to 20 mA/cm^2, the cycling stability is 72% after 2000 cycles at a high current density of 10 mA/cm^2, and the high specific energy density is 166.7 Wh/kg at a current density of 2 mA/cm^2 in a two-electrode system.

Keywords: $ZnCo_2O_4/Ni(OH)_2$, Composite Electrodes, Specific Capacitance, Specific Energy Density, Specific Power Density.

[*]Corresponding author email: xtzhangzhang@hotmail.com

1. Introduction

The concerns over environmental pollution and depletion of fossil fuels have evoked unprecedented endeavor in developing clean, efficient and renewable energy sources to maintain a healthy, prompt and sustainable economic development. Indeed, the development has led to a rapid increase of green energy production such as solar and wind resources. However, the solar and wind resources are unstable and intermittent, meaning that energy storage systems must be developed to store the electrical energy generated from these sources.[1-6] Among various energy storage systems, batteries and supercapacitors are the most promising ones to bridge the gap between the growing economic problems and increasing energy demand.[7] Especially, supercapacitors have many advantages over batteries, including high power density, fast charging/discharging rate, and excellent cycle stability, which makes them desirable for a range of applications, from electric devices to smart grid.[8-13]

Supercapacitors can be divided into electrical double layer capacitors and pseudocapacitors (PCs), according to the charge storage mechanisms.[14] In particularly, PCs arising from the fast reversible Faradic redox reactions at the electrode surface usually provide much higher specific capacitance than supercapacitors made of carbonaceous materials based on electric double layer charge storage.[15-19] Therefore, most of current researches have been focused on PCs. Transition metal oxides and hydroxides have been found to be excellent electrode materials for high performance PCs due to their variety of oxidation states for charge transfer. Among them, $Ni(OH)_2$ is an especially attractive transition hydroxides for electrodes because of its high theoretical specific capacitance, well-defined electrochemical redox activity and low cost.[20-23] However, its rate capability and cycle stability are largely unsatisfactory. For example, Yang et al.[22] synthesized α-$Ni(OH)_2$ electrode materials with ultrahigh capacitance of 3152 F/g at a current density of 4 A/g, in which α-$Ni(OH)_2$ was electrodeposited on Ni foam, a high electrical conductivity and 3D structure serves as a current collector to facilitate electron transfer and ion diffusion for an enhanced

capacity performance. But its poor cycling stability was presented due to the weak adherent force between $Ni(OH)_2$ and the substrate. Fortunately, some high-performance results have been achieved recently. For instance, Wang et al.[24] produced $Ni(OH)_2$ nanoflakes on multi-layer graphite nanosheets, exhibiting not only high specific capacitance but also remarkable rate capability and excellent cycling stability, which can be attributed to the large active surface area and good electrical connection between substrate and electrode materials for fast redox reactions. Jiang et al.[25] synthesized uniform $Ni(OH)_2$ hierarchical nanostructures consisting of ultrathin nanoflakes with thickness of 7.4 nm, which exhibits high specific capacitance, high rate capability and good cycling stability. The good performance can be attributed to the larger surface area produced by decreasing the particle size, thus improving the electrode/electrolyte contact area, shortening the diffusion path of carriers and enhancing the electron transporting in electrodes. Therefore, to optimize the electrochemical properties of $Ni(OH)_2$, increasing its surface area and providing reliable electrical conductivity pathway become essential criteria in designing high-performance electrodes for $Ni(OH)_2$-based electrochemical supercapacitors. One promising route to realize the practical application of $Ni(OH)_2$ and enhance its electrical conductivity is to grow $Ni(OH)_2$ nanostructures onto highly conductive backbones. This method yields a highly electrolytic accessible surface area of active $Ni(OH)_2$ electrode materials and also improves the electrical conductivity of $Ni(OH)_2$ electrode materials. And a few recent reports have proved the correctness of this design. For example, Huang et al.[26] prepared $NiCo_2O_4/Ni(OH)_2$ on carbon fiber paper, which exhibits high capacitance performance and good rate capability. Zhou et al.[27] synthesized $Ni_3S_2/Ni(OH)_2$ with high specific capacitance and good cycling performance. Recent studies prove that $ZnCo_2O_4$ which has been widely investigated for application in the areas of high-performance Li-ion batteries, electrocatalysts and gas sensors, also exhibits excellent electrochemical performance. For example, $ZnCo_2O_4$ nanowire arrays on Ni foam reported by Wang et al.[28] obtained high specific capacitance (1625 F/g at 5 A/g), excellent rate capability (59% capacitance retention at 80 A/g) and good cycling stability (94% capacitance retention over 5000 cycles).

$ZnCo_2O_4$ nanorods on Ni foam prepared by Liu et al. [29] presented high specific capacitance (1400 F/g at 1 A/g), excellent rate capability (72.5% capacity retention at 20 A/g) and good cycling stability 97% after 1000 cycles at 6 A/g). $ZnCo_2O_4$ nanowire cluster arrays on Ni foam synthesized by Guan et al.[30] exhibited high specific capacitance of 1620 F/g at 8 A/g and excellent cycling ability of 90% after 6000 cycles at various current densities up to 100 mA/cm^2. According to the review above, $ZnCo_2O_4$ could produce high specific capacitance comparable to other ternary metal oxides which have attracted great attention in the field of supercapacitor such as $NiCo_2O_4$, $NiMoO_4$. Moreover, it has much better rate capacitance and cycle stability. The excellent performance of $ZnCo_2O_4$ is inseparable from its good electrical conductivity. In this regard, the composite electrodes consisting of $ZnCo_2O_4$ and $Ni(OH)_2$ nanostructures can be an effective strategy of producing outstanding PCs. So, in this work, the hierarchical $ZnCo_2O_4$/$Ni(OH)_2$ nanostructures on Ni foam were rationally designed and successfully developed by growing $Ni(OH)_2$ nanosheets on highly porous $ZnCo_2O_4$ nanowires. This electrode design has many apparent advantages as follows: (1) Both of the two nanostructure materials are promising pseudocapacitive electrode materials, which undergo redox reactions with cations and anions in the electrolyte, hence contributing to the total capacitance. (2) The highly porous $ZnCo_2O_4$ nanowires with good electrical conductivity directly grown on conductive Ni foam can enhance the adherent force between electrode materials and current collector, and act both as the backbone and electron "superhighway" for charge storage and delivery, overcoming the intrinsic poor conductivity of $Ni(OH)_2$ itself, and the highly porous feature provides a large electrode/electrolyte contact interface. (3) The $Ni(OH)_2$ nanosheets growing onto the $ZnCo_2O_4$ nanowires greatly enhances the surface area, providing more electroactive sites for Faradaic reaction. (4) The abundant space between individual nanostructures allows for facile diffusion of electrolyte into inner region of the electrode, leading to a high utilization of the electrode materials. (5) The direct growth of composite nanostructures on Ni foam as the current collector ensures good mechanical adhesion and electric connection of the electrode materials to the current collector, avoiding the use of polymer binder and

conducting additives, improving the utilization of the electrode materials. Benefiting from the multiple apparent advantages of this configuration, the as-prepared hierarchical $ZnCo_2O_4/Ni(OH)_2$ composite electrodes exhibit high electrochemical performance which would hold great promise for high-performance energy storage applications.

2. Experimental details

2.1. Materials synthesis

All the reagents used in the experiments were of analytical grade and used without further purification.

Synthesis of $ZnCo_2O_4$ nanowires: Prior to the synthesis, the Ni foam (1 cm×1 cm) was treated with 6 M HCl for 10 min to remove the oxide layer and then washed thoroughly with deionized water. The $ZnCo_2O_4$ nanowires growing on Ni foam were realized by a facile hydrothermal method. In a typical synthesis, 1 mmol $Zn(NO_3)_2$, 2 mmol $Co(NO_3)_2$, 2 mmol NH_4F, and 5 mmol urea were dissolved in 40 mL deionized water under constant magnetic stirring to form a clear red solution. The solution and a piece of pretreated Ni foam were transferred to a 50 mL Teflon-lined stainless steel autoclave, heated in an oven at 120 ^oC for 5 h and then cooled down to room temperature naturally. The Ni foam coated with the precursor was rinsed with deionized water, followed by annealing at 400 ^oC in air for 2 h.

Synthesis of hierarchical $ZnCo_2O_4/Ni(OH)_2$ nanostructures: Hierarchical $ZnCo_2O_4/Ni(OH)_2$ nanostructures were obtained by electrodeposition, which was conducted in a 100 mL of solution containing 0.5 g $Ni(NO_3)_2$ at -1.0 V for 300 s at room temperature. Pure $Ni(OH)_2$ nanosheets were deposited on Ni foam for 600 s in order to have the same weight with the $ZnCo_2O_4/Ni(OH)_2$ composite nanostructures.

2.2. Materials Characterization

The morphology and structure of the as-synthesized composites were characterized by scanning electron microscopy (SEM, Hitachi SU 70) equipped with energy dispersive X-ray spectrometer (EDX). Transmission electron microscopy (TEM; FEI, Tecnai TF 20) and X-ray diffraction (XRD; Dlmax 2600, Rigaku, Japan) using the Cu Kα radiation (λ = 1.5418 Å).

2.3. Electrochemical Measurements

A three-electrode cell was used for electrochemical measurements on a Biologic electrochemical workstation with the as-prepared samples as working electrode, a Pt foil and Hg/HgO as the counter and reference electrodes, respectively. 3.0 M KOH aqueous solution was used as the electrolyte. Cyclic voltammetry (CV) tests were performed at a scanning rate of 15, 25, 50, and 100 mV/s, and potential window from 0 to 0.7 V at room temperature. The galvanostatic charge-discharge tests were conducted at 2, 5, 10, 15, and 20 mA/cm^2. Electrochemical impedance spectroscopy (EIS) measurements were carried out on this apparatus in the frequency range of 100 kHz to 10 Hz.

The specific capacitance (C_s), area capacitance (C_a), specific energy density (E) and specific power density (P) of the electrodes can be calculated according to the following equation respectively:

$$C_s = \frac{I\Delta t}{m\Delta V} \quad (1)$$

$$C_a = \frac{I\Delta t}{SV} \quad (2)$$

$$E = \frac{C_s \Delta V^2}{2} \quad (3)$$

$$P = \frac{E}{\Delta t} \quad (4)$$

where C (F/g) is the specific capacitance of the electrode materials, I(A) is the current during the discharge process, Δt (s) is the discharge time, ΔV(V) is the potential window and m (g) is the mass of the electrode materials.

3. Results and discussion

The morphologies of the $ZnCo_2O_4$ nanowires and $ZnCo_2O_4/Ni(OH)_2$ composite nanostructures on Ni foam are shown in Fig. 1. Fig. 1a shows the high-density $ZnCo_2O_4$ nanowires grown on the whole Ni foam. The magnified SEM image in Fig. 1b clearly reveals that the nanowires have an average diameter of 100 nm and length of up to 5 μm. The further magnified view in the inset shows the porous structure of $ZnCo_2O_4$ nanowires, which was formed due to the release of gaseous species during the calcining process.[28,31-32] Fig. 1c displays a low-magnification SEM image of hierarchical $ZnCo_2O_4/Ni(OH)_2$ composite nanostructures after electrodeposition. It shows that the integration of $Ni(OH)_2$ nanomaterials into the mesoporous $ZnCo_2O_4$ nanowires does not worsen the ordered structure. Fig. 1d shows the high-magnification SEM image. Obviously, no $Ni(OH)_2$ is packed in the interspace of the nanowires, suggesting that the $Ni(OH)_2$ nanosheets are preferentially deposited on the surface of $ZnCo_2O_4$ nanowires. Therefore, the uniform coverage of $Ni(OH)_2$ nanosheets on the surface of individual $ZnCo_2O_4$ nanowires can be seen. Such a unique hierarchical nanostructure has open and free interspaces among themselves, which assures that electrolytes are highly accessible to all the electrode materials and then could improve the utilization rate of electrode materials.

A typical XRD pattern of the as-synthesized nanostructures is shown in Fig. 2. To avoid the effect of the nickel foam, the sample was scratched from the nickel foam. All the diffraction peaks can be readily indexed to face-centered cubic $ZnCo_2O_4$ (JCPDS card no. 23-1390). While the presence of $Ni(OH)_2$ was not confirmed by the

XRD pattern due to its trace amount. The presence of $Ni(OH)_2$ can be verified by HRTEM image.

The microstructures of the $ZnCo_2O_4$ and hierarchical $ZnCo_2O_4/Ni(OH)_2$ composite nanostructures were further investigated using TEM. Fig. 3a shows the typical TEM image of a $ZnCo_2O_4$ nanowire, confirming further formation of the highly porous structure, which is consistent with SEM observation. Fig. 3b shows a HRTEM image of the porous $ZnCo_2O_4$ nanowire. The interplanar spacing is calculated to be 0.29 nm and 0.25 nm, respectively, corresponding to the (220) and (311) lattice planes. The typical TEM image of the $ZnCo_2O_4/Ni(OH)_2$ composite nanostructure is shown in Fig. 3c. It is evidently observed that the mesoporous $ZnCo_2O_4$ is totally covered by $Ni(OH)_2$ nanosheets, forming a typical hierarchical nanostructure. The HRTEM examination shown in Fig. 3d reveals an interplanar spacing of 0.23 nm and 0.27 nm, corresponding to the (002) and (100) plane of $Ni(OH)_2$.

The pseudocapacitive performance of the hierarchical $ZnCo_2O_4/Ni(OH)_2$ composite nanostructures were investigated to highlight the benefits of the unique architecture in a three-electrode configuration with 3 M KOH as the electrolyte. Fig. 4a shows the CV curves of the $ZnCo_2O_4/Ni(OH)_2$ composite nanostructures supported on Ni foam at a scan rate of 15, 25, 50, and 100 mV/s, respectively. A couple of redox peaks are visible in the CV curves within the potential window from 0 to 0.7 V (vs. Hg/HgO), indicating the pseudocapacitance nature of the as-synthesized electrode materials. Interestingly, the redox current almost linearly increases with increasing scan rate, demonstrating that the kinetics of interfacial Faradic redox reactions and the rate of electronic and ionic transport are rapid enough.[33-34] And also, the reduction and oxidation peaks slightly shift toward lower and higher potential, respectively, which can be attributed to the polarization effect of the electrode.[35-36] Moreover, the CV curves still keep the original shape even at large scan rate of 100 mV/s, revealing the favorable electron and ionic conduction and indicating the excellent high-rate performance of the hierarchical nanostructures.

Galvanostatic charge-discharge measurements were further performed in the voltage range between 0 and 0.5 V (vs. Hg/HgO) to estimate the capacitance of the electrode materials. As shown in Fig. 4b, all of the curves have the obvious voltage plateaus in the charge and discharge process. The potential plateaus observed in the discharge curves correspond to the reductive process and match well with the reduction peaks observed in the CV curves, indicating good pseudocapacitive behaviors. The specific capacitances are calculated to be 2826, 2723, 2540, 2305, and 2019 F/g at current densities of 2, 5, 10, 15, and 20 mA/cm^2, respectively, according to formula (1). The specific capacitance value reported here (2540 F/g at 10 mA/cm^2) is superior to most other previously reported core/shell nanoarchitectures, such as Co_3O_4/$NiMoO_4$ core/shell nanowire arrays (1230 F/g at 10 mA/cm^2)[37], $NiCo_2O_4$/$CoMoO_4$ (1347.3 F/g at 10 mA/cm^2)[38], proving the great advantages of the present composite nanostructures. The corresponding areal capacitances are 2.8, 2.7, 2.5, 2.3, and 2.0 F/cm^2, respectively, according to formula (2). Even at a high current density of 20 mA/cm^2, the specific capacitance still remains at 2019 F/g, 71.4% of that at a current density of 2 mA/cm^2, highlighting the excellent rate capability.

To evaluate the benefits of the hierarchical $ZnCo_2O_4$/$Ni(OH)_2$ composite nanostructures superior to the corresponding single oxide, the bare $ZnCo_2O_4$ nanowires and $Ni(OH)_2$ nanosheets with the same weight of $ZnCo_2O_4$/$Ni(OH)_2$ composite nanostructures were also characterized. Fig. 5a shows the CVs collected from $ZnCo_2O_4$, $Ni(OH)_2$, and $ZnCo_2O_4$/$Ni(OH)_2$ at a scan rate of 15 mV/s. Apparently, a pair of weak redox peaks are observed for the $ZnCo_2O_4$ nanowire electrodes. The CV curve of $Ni(OH)_2$ exhibits a pair of strong redox peaks, indicating that the capacitance characteristics are primarily governed by Faradaic reactions. From the CV curve of the composite electrode, it could be observed that both the position and intensity of redox peaks for $ZnCo_2O_4$/$Ni(OH)_2$ lie in between those for $Ni(OH)_2$ and $ZnCo_2O_4$. In addition, from the area integrated within the current-potential curves, it could be deduced that both the $ZnCo_2O_4$ and $Ni(OH)_2$ electrodes all contribute to the total capacitance of $ZnCo_2O_4$/$Ni(OH)_2$ composite electrodes. As shown in Fig. 5b,

galvanostatic charge-discharge measurements of $ZnCo_2O_4$, $Ni(OH)_2$ and $ZnCo_2O_4/Ni(OH)_2$ electrodes were further performed at the current density of 2 mA/cm^2. From Fig. 5b, the specific capacitances of the composite electrodes, $ZnCo_2O_4$ nanowire electrodes and $Ni(OH)_2$ nanosheet electrodes are calculated to be 2826 F/g, 1227 F/g, and 1476 F/g, respectively. In addition, the CV and galvanostatic charge-discharge curves of the two individual oxide electrodes at various scan rates and current densities are also measured to compare the rate capability of the three electrodes in Figure S1 and Figure S2. Their specific capacitances calculated from each discharge curve are as shown in Figure. 5c. It is worth noted that the capacitance retention is 67%, 33%, and 71.4% as the current density is increased from 2 to 20 mA/cm^2 for $ZnCo_2O_4$, $Ni(OH)_2$, and $ZnCo_2O_4/Ni(OH)_2$. The rate capability of composite electrodes from 2 to 20 mA/cm^2 (2 to 20 A/g) is a little better than many other pseudocapacitor electrodes such as $Ni_3S_2/Ni(OH)_2$ (38% capacitance retention from 5.1 A/g to 19.8 A/g)[27], $NiCo_2O_4/MnO_2$ (50% capacitance retention from 2 mA/cm^2 to 20 mA/cm^2)[39]. Such good rate capability of hierarchical $ZnCo_2O_4/Ni(OH)_2$ composite nanostructures can be mainly ascribed to the enhanced adherent force between electrode materials and Ni foam by means of $ZnCo_2O_4$ nanowires.

Another important requirement for supercapacitor applications is cycling stability. The long-term cycling stability over 2000 cycles for the three electrodes at a current density of 10 mA/cm^2 were carried out using galvanostatic charge/discharge cycling techniques in the potential window from 0 to 0.5 V. Fig. 5d shows the specific capacitance retention of the $ZnCo_2O_4$, $Ni(OH)_2$ and $ZnCo_2O_4/Ni(OH)_2$ as a function of charging/discharging cycling numbers. The $ZnCo_2O_4$ nanowire electrodes display almost no decay of capacitance. This good cycling performance is in accordance with previously reported cycling stability of $ZnCo_2O_4$. The pure $Ni(OH)_2$ electrodes exhibit 25% capacitance retention. Impressively, the $ZnCo_2O_4/Ni(OH)_2$ composite electrodes display 72% capacitance retention after 2000 cycles which is impressively superior to that of $Ni(OH)_2$ nanosheets and is better than the reported cycling stability of $NiCo_2O_4/Ni(OH)_2$ (dropped over 64% after 1000 cycles at a low current density of 5

mA/cm^2)[24]. Furthermore, the shape of charge-discharge curves for the last 10 cycles remained the same as that for the first 10 cycles (Figure S3), illustrating the excellent long-term cycle stability of the composite electrode.

Specific energy and specific power are two key factors to evaluate the power applications of electrochemical supercapacitors. A good supercapacitor is expected to provide high energy density or high specific capacitance at high current densities. Meanwhile, the two-electrode supercapacitor geometry has been suggested to be the best indication of an electrode material's performance.[40] Figure 6a represents scan rate dependence on the $ZnCo_2O_4$/$Ni(OH)_2$ voltammograms in two-electrode system in a potential window of -0.6 V to +0.6 V. The reduction and oxidation peaks on CV curves can be observed and the peak current becomes larger and larger with the increasing scan rate, in agreement with the trend revealed by the three-electrode system. Galvanostatic charge-discharge measurements at different current densities were conducted and the resultant profiles are given in Figure 6b. Charge and discharge plateaus are clearly observed for each curve, indicating good pseudocapacitive behavior, which is also confirmed by its CV curves. The energy density and the power density were calculated from the discharge curves using formulas (3) and (4), respectively. The CVs and galvanostatic charge and discharge curves of $ZnCo_2O_4$ and $Ni(OH)_2$ were also tested in two-electrode system for comparison (Figure S4 and Figure S5). Figure 6c depicts the Ragone plots of the $ZnCo_2O_4$, $Ni(OH)_2$, and $ZnCo_2O_4$/$Ni(OH)_2$ electrodes, in which the $ZnCo_2O_4$/$Ni(OH)_2$ composite electrodes obviously show the best energy density and power density performance. The specific energy density decreases from 166.7 to 98.4 Wh/kg when the current density increases from 2 to 20 mA/cm^2, while the power density increases from 1.2 kW/kg to 12 kW/kg. These values are remarkable compared to the most reported electrode materials, such as $ZnCo_2O_4$ electrode[28] with energy density of 12.5 Wh/kg when power density is 0.8 kW/kg at 1.2 mA/cm^2, Co_2O_3/$Ni(OH)_2$ electrode[41] with energy density of 41.9 Wh/kg when power density is 36.10 W/kg at 2.5 mA/cm^2, $NiCo_2O_4$/$CoMoO_4$ electrode[38] with energy density of 64.9 Wh/kg when power density

is 322 W/kg at 10 mA/cm^2, $NiCo_2O_4/Co_xNi_{1-x}(OH)_2$ electrode[42] with energy density of 31.2 Wh/kg when power density is 396 W/kg at 5 mA/cm^2, demonstrating the capability of $ZnCo_2O_4/Ni(OH)_2$ composite electrodes for electrochemical supercapacitors in hybrid vehicle systems.

Compared with $ZnCo_2O_4$ and $Ni(OH)_2$ electrodes, the $ZnCo_2O_4/Ni(OH)_2$ composite electrodes show a better performance in terms of specific capacitance, specific energy density, specific power density and rate capability. In order to clarify the reason, the EIS spectra were measured in Fig. 7. The internal resistances (R_b) at the high-frequency intercept of the real axis was measured to be 0.36, 0.4, and 0.55 Ω for $ZnCo_2O_4$, $ZnCo_2O_4/Ni(OH)_2$, and $Ni(OH)_2$ respectively. The slight increase of $ZnCo_2O_4/Ni(OH)_2$ for the internal resistances compared to $ZnCo_2O_4$ is probably attributed to the low electrical conductivity of the $Ni(OH)_2$.[43] The charge transfer resistance (R_{ct}), which results from diffusion of electrons, can be calculated from the diameter of the semicircle in the high frequency range. The R_{ct} of the $ZnCo_2O_4/Ni(OH)_2$ is obviously smaller than that of the bare $ZnCo_2O_4$ and $Ni(OH)_2$, implying that the composite electrode provides a better pathway for ion transfer and electron transport. In the low frequency area, the slope of the curve shows the Warburg resistance (Z_w) which represents the electrolyte diffusion to the electrode surface.[44-45] The $ZnCo_2O_4/Ni(OH)_2$ composite electrode has a more ideal straight line, indicating more efficient electrolyte diffusion. All of these demonstrate the good electrochemical activity of $ZnCo_2O_4/Ni(OH)_2$ composite electrodes for energy storage.

According to the results above, the good electrochemical performances of the hierarchical $ZnCo_2O_4/Ni(OH)_2$ composite electrodes can be attributed to the four reasons below: (1) As is well known, both $ZnCo_2O_4$ and $Ni(OH)_2$ are promising pseudocapacitive electrode materials. (2) The $Ni(OH)_2$ nanosheets growing onto the $ZnCo_2O_4$ nanowires. Here $ZnCo_2O_4$ nanowires act as the backbone and electron "superhighway" for charge storage and delivery. The backbone improves the

conductivity of $Ni(OH)_2$ itself, greatly enhances the surface area of the $Ni(OH)_2$ nanosheets, and provides more electroactive sites for Faradaic reaction. (3) On the other hand, $ZnCo_2O_4$ nanowires play an important role in solidifying electrode materials to Ni foam as current collector, which avoids electrode materials falling off. (4) $ZnCo_2O_4$ and $Ni(OH)_2$ composite electrodes are rationally designed.

4. Conclusions

$ZnCo_2O_4/Ni(OH)_2$ composite electrodes are synthesized on Ni foam. They exhibit high electrochemical performance, with a large specific capacitance of 2826 F/g at 2 mA/cm^2 and a high energy density of 166.7 Wh/kg at a power density of 1.2 kW/kg. When the current density increases from 2 to 20 mA/cm^2, the capacitance retention is 71.4%, indicating a good rate capability. Impressively, the $ZnCo_2O_4/Ni(OH)_2$ composite electrodes exhibit a high specific capacitance retention of 72% after 2000 cycles at a high current density of 10 mA/cm^2, indicating good cycling stability. These results demonstrate that the hierarchical $ZnCo_2O_4/Ni(OH)_2$ composite electrodes would hold great promise for high performance supercapacitor applications.

Acknowledgments

This work was partially supported by the Natural Science Foundation of China (No. 51172058 and 51472066), the Key Project of Natural Science Foundation of Heilongjiang Province (ZD201112 and A201007), and Institution of Higher Education, Doctoral Fund Jointly Funded Project (20112329110001), and the Graduate Students' Scientific Research Innovation Project of Heilongjiang Province (HSDSSCX2014-05).

References

1 G. P. Wang, L. Zhang and J. J. Zhang, *Chem. Soc. Rev.*, 2012, **41**, 797-828.

2 J. P. Liu, J. Jiang, M. Bosman and H. J. Fan, *J. Mater. Chem.*, 2012, **22**, 2419-2446.

3 H. Jiang, J. Ma and C. Z. Li, *Chem. Commun.*, 2012, **48**, 4465-4467.

4 L. F. Chen, Z. H. Huang, H. W. Liang, W. T. Yao and S. H. Yu, *Energy Environ. Sci.*, 2013, **6**, 3331-3338.

5 D. Tang, J. Liu, X. Y. Wu, R. H. Liu, X. Han, Y. Z. Han, H. Huang, Y. Liu and Z. H. Kang, *ACS Appl. Mater. Interfaces*, 2014, **6**, 7918-7925.

6 D. Tang, Y. Z. Han, W. B. Ji, S. Qiao, X. Zhou, R. H. Liu, X. Han, H. Huang, Y. Liu and Z. H. Kang, *Dalton Trans*, 2014, **43**, 15119-15125.

7 P. Simon and Y. Gogotsi, *Nature Mater.*, 2008, **7**, 845-854.

8 M. Huang, Y. X. Zhang, F. Li, L. L. Zhang, Z. Y. Wen and Q. Liu, *J. Power Sources*, 2014, **252**, 98-106.

9 X. Xiao, T. P. Ding, L. Y. Yuan, Y. Q. Shen, Q. Z. Zhong, X. H. Zhang, Y. Z. Cao, B. Hu, T. Zhai, L. Gong, J. Chen, Y. X. Tong, J. Zhou and Z. L. Wang, *Adv. Energy Mater.*, 2012, **2**, 1328-1332.

10 G. Q. Zhang, H. B. Wu, H. E. Hoster, M. B. Chan-Park and X. W. Lou, *Energy Environ. Sci.*, 2012, **5**, 9453-9456.

11 X. Xiao, X. Peng, H. Jin, T. Li, C. Zhang, B. Gao, B. Hu, K. Huo and J. Zhou, *Adv. Mater.*, 2013, **25**, 5091-5097.

12 F. X. Wang, S. Y. Xiao, Y. Y. Hou, C. L. Hu, L. L. Liu and Y. P. Wu, *RSC Adv.*, 2013, **3**, 13059-13084.

13 G. H. Yu, X. Xie, Z. N. Bao and Y. Cui, *Nano Energy.*, 2013, **2**, 213-234.

14 M. Winter and R.J. Brodd, *Chem. Rev.*, 2004, **104**, 4245-4269.

15 W. J. Zhou, X. Cao, Z. Y. Zeng, W. H. Shi, Y. Y. Zhu, Q. Y. Yan, H. Liu and H. Zhang, *Energy Environ. Sci.*, 2013, **6**, 2216-2221.

16 L. Huang, D. C. Chen, Y. Ding, S. Feng, Z. L. Wang and M. L. Liu, *Nano Lett.*, 2013, **13**, 3135-3139.

17 L. Yang, S. Cheng, Y. Ding, X. B. Zhu, Z. L. Wang and M. L. Liu, *Nano Lett.*, 2012, **12**, 321-325.

18 H. L. Wang, H. S. Casalongue, Y. Y. Liang and H. J. Dai, *J. Am. Chem. Soc.*, 2010, **132**, 7472-7477.

19 Z. S. Wu, D. W. Wang, W. Ren, J. Zhao, G. Zhou, F. Li and H. M. Cheng, *Adv. Funct. Mater.*, 2010, **20**, 3595-3602.

20 G. X. Hu, C. X. Li and H. Gong, *J. Power Sources*, 2010, **195**, 6977-6981.

21 H. L. Wang, H. S. Casalongue, Y. Y. Liang and H. J. Dai, *J. Am. Chem. Soc.*, 2010, **132**, 7472-7477.

22 G. W. Yang, C. L. Xu and H. L. Li, *Chem. Commun.*, 2008, **48**, 6537-6539.

23 W. Zhou, M. Yao, L. Guo, Y. M. Li, J. H. Li and S. H. Yang, *J. Am. Chem. Soc.*, 2009, **131**, 2959-2964.

24 X. Wang, Y. Y. Wang, C. M. Zhao, Y. X. Zhao, B. Y. Yan and W. T. Zheng, *New J. Chem.*, 2012, **36**, 1902-1906.

25 H. Jiang, T. Zhao, C. Z. Li and J. Ma, *J. Mater. Chem.*, 2011, **21**, 3818-3823.

26 L. Huang, D. C. Chen, Y. Ding, Z. L. Wang, Z. Z. Zeng and M. L. Liu, *ACS Appl. Mater. Interfaces*, 2013, **5**, 11159-11162.

27 W. J. Zhou, X. H. Cao, Z. Y. Zeng, W, H. Shi, Y. Y. Zhu, Q. Y. Yan, H. Liu, J. Y. Wang and H. Zhang, *Energy Environ. Sci.*, 2013, **6**, 2216-2221.

28 S. B. Wang, J. Pu, Y. Tong, Y. Y. Chen, Y. Gao and Z. H. Wang, *J. Mater. Chem. A.*, 2014, **2**, 5434-5440.

29 B. Liu, B. Y. Liu, Q. F. Wang, X. F. Wang, Q. Y. Xiang, D. Chen and G. Z. Shen, *ACS Appl. Mater. Interfaces.*, 2013, **5**, 10011-10017.

30 B. K. Guan, D. Guo, L. L. Hu, G. H. Zhang, T. Fu, W. J. Ren, J. D. Li and Q. H. Li, *J. Mater. Chem. A*, 2014, **2**, 16116-16123.

31 K. B. Xu, R. J. Zou, W. Y. Li, Y. F. Xue, G. S. Song, Q. Liu, X. J. Liu and J. Q. Hu, *J. Mater. Chem. A*, 2013, **1**, 9107-9113.

32 R. B. Rakhi, W. Chen, D. Cha and H. N. Alshareef, *Nano Lett.*, 2012, **12**, 2559-2567.

33 X. J. Ma, L. B. Kong, W. B. Zhang, M. C. Liu, Y. C. Luo and L. Kang, *RSC Adv.*, 2014, **4**, 17884-17890.

34 L. B. Kong, J. W. Lang, M. C. Liu, Y. C. Luo and L. Kang, *J. Power Sources*, 2009, **194**, 1194-1201.

35 D. P. Cai, D. D. Wang, B. Liu, L. L. Wang, Y. Liu, H. Li, Y. R. Wang, Q. H. Li and T. H. Wang, *ACS Appl. Mater. Interfaces*, 2014, **6**, 5050-5055.

36 J. Yan, Z. Fan, W. Sun, C. Ning, T. Wei, Q. Zhang, R. Zhang, L. Zhi and F. Wei, *Adv. Funct. Mater.*, 2012, **22**, 2632-2641.

37 D. P. Cai, D. D. Wang, B. Liu, L. L. Wang, Y. Liu, H. Li, Y. R. Wang, Q. H. Li and T. H. Wang, *ACS Appl. Mater. Interfaces*, 2014, **6**, 5050-5055.

38 D. P. Cai, B. Liu, D. D. Wang, L. L. Wang, Y. Liu, H. Li, Y. R. Wang, Q. H. Li and T. H. Wang, *J. Mater. Chem. A.*, 2014, **2**, 4954-4960.

39 L. Yu, G. Q. Zhang, C. Z. Yuan and X. W. Lou, *Chem. Commun.*, 2013, **49**, 137-139.

40 M. D. Stoller and R. S. Ruoff, *Energy Environ. Sci.*, 2010, **3**, 1294-1301.

41 C. H. Tang, X. S. Yin and H. Gong, *ACS Appl. Mater. Interfaces*, 2013, **5**, 10574-10582.

42 K. B. Xu, R. J. Zou, W. Y. Li, Q. Liu, X. J. Liu, L. An and J. Q. Hu, *J. Mater. Chem. A*, 2014, **2**, 10090-10097.

43 D. Guo, H. M. Zhang, X. Z. Yu, M. Zhang, P. Zhang, Q. H. Li and T. H. Wang, *J. Mater. Chem. A*, 2013, **1**, 7247-7254.

44 X. Y. Liu, S. J. Shi, Q. Q. Xiong, L. Li, Y. J. Zhang, H. Tang, C. D. Gu, X. L. Wang and J. P. Tu, *ACS Appl. Mater. Interfaces*, 2013, **5**, 8790-8795.

45 W. Y. Li, G. Li, J. Q. Sun, R. J. Zou, K. B. Xu, Y. G. Sun, Z. G. Chen, J. M. Yang and J. Q. Hu, *Nanoscale*, 2013, **5**, 2901-2908.

Figure Captions:

Fig. 1. (a) Low and (b) high-magnification SEM images of $ZnCo_2O_4$ nanowires. (c) Low and (d) high-magnification SEM images of hierarchical $ZnCo_2O_4/Ni(OH)_2$ nanostructures.

Fig. 2. XRD pattern of the $ZnCo_2O_4$ nanowires grown on Ni foam.

Fig. 3. (a) TEM and (b) HRTEM images of the $ZnCo_2O_4$ nanowires. (c) TEM and (d) HRTEM images of the hierarchical $ZnCo_2O_4/Ni(OH)_2$ nanostructures.

Fig. 4. Electrochemical characterization of $ZnCo_2O_4/Ni(OH)_2$ composite electrodes. (a) CV curves of $ZnCo_2O_4/Ni(OH)_2$ composite electrodes at various scan rates. (b) Galvanostatic charge-discharge curves of $ZnCo_2O_4/Ni(OH)_2$ composite electrodes at various current densities.

Fig. 5. (a) CV and (b) galvanostatic charge-discharge curves for as-synthesized $ZnCo_2O_4$ nanowire electrodes, $Ni(OH)_2$ nanosheet electrodes and $ZnCo_2O_4/Ni(OH)_2$ composite electrodes, recorded at a scan rate of 15 mV/s and at a current density of 2 mA/cm^2, respectively. (c) Specific capacitances for $ZnCo_2O_4$, $Ni(OH)_2$, $ZnCo_2O_4/Ni(OH)_2$ as a function of the current density. (d) Cycling performances of $ZnCo_2O_4$, $Ni(OH)_2$ and $ZnCo_2O_4/Ni(OH)_2$ during 2000 cycles at a current density of 10 mA/cm^2.

Fig. 6. (a) CV and (b) galvanostatic charge-discharge curves of $ZnCo_2O_4/Ni(OH)_2$ composite electrodes at various scan rates and current densities in a two electrode system, respectively.

Fig. 7. EIS spectra of the $ZnCo_2O_4$ nanowires, $Ni(OH)_2$ nanosheets and $ZnCo_2O_4/Ni(OH)_2$ composite nanostructures. Inset shows the magnification part of high frequency range for the EIS spectra.

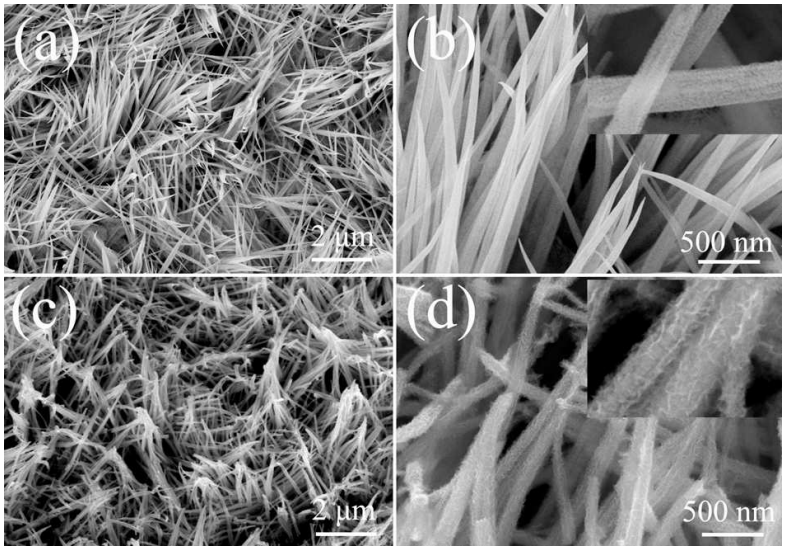

Figure 1 by H. X. Chuo, et al.

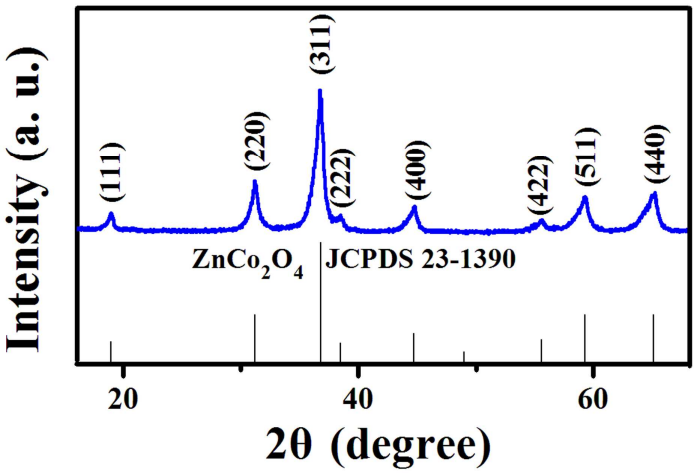

Figure 2 by H. X. Chuo, et al.

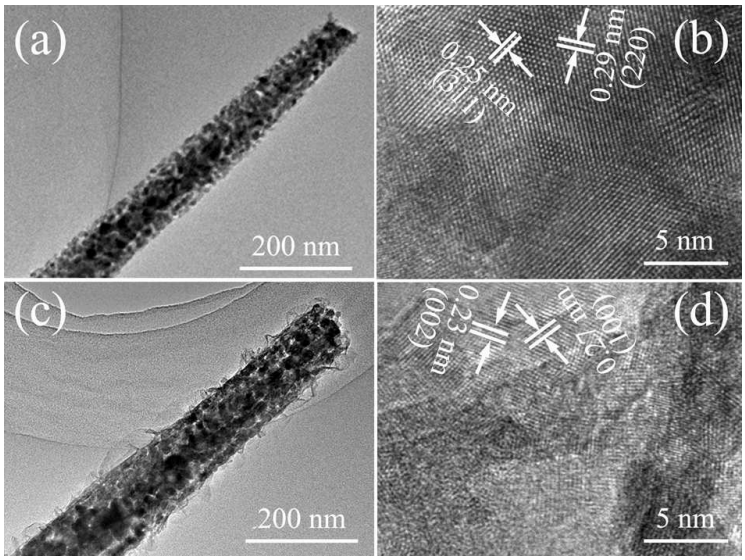

Figure 3 by H. X. Chuo, et al.

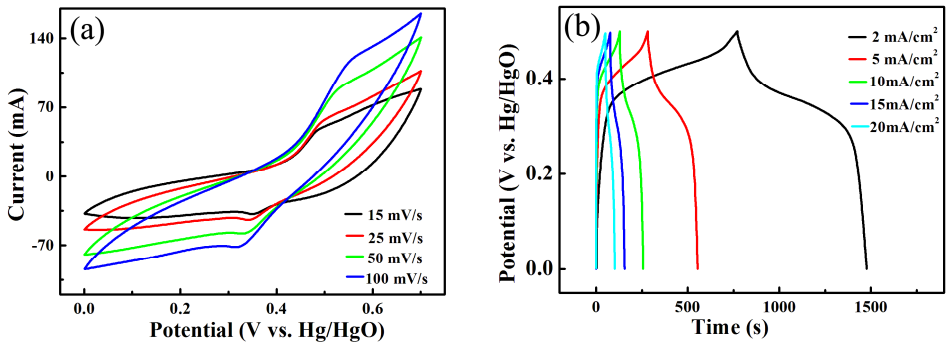

Figure 4 by H. X. Chuo, et al.

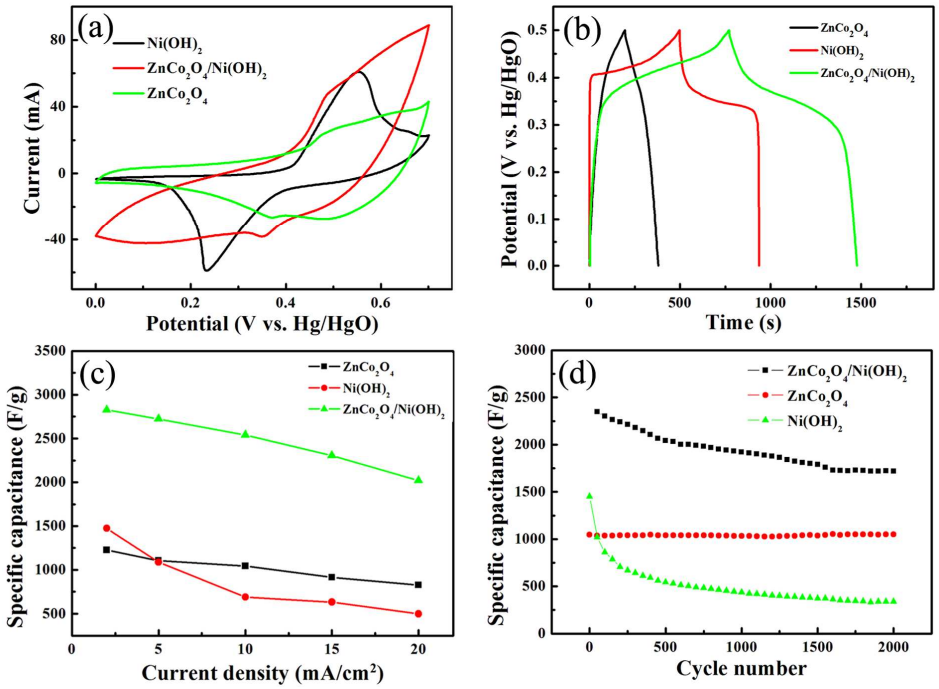

Figure 5 by H. X. Chuo, et al.

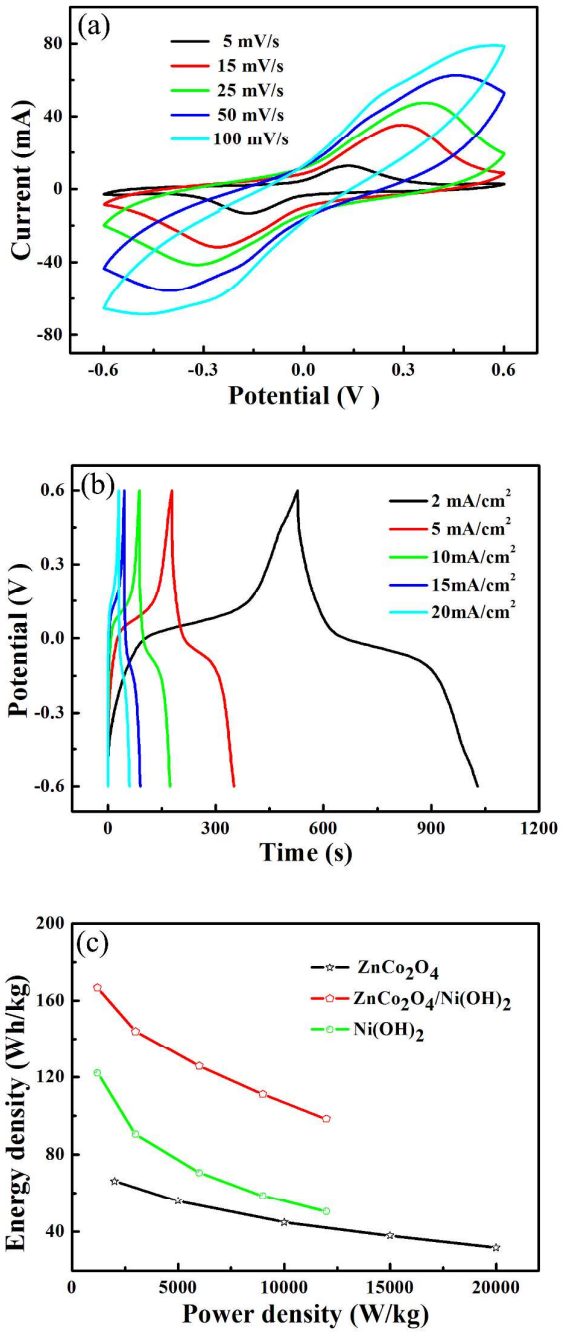

Figure 6 by H. X. Chuo, et al.

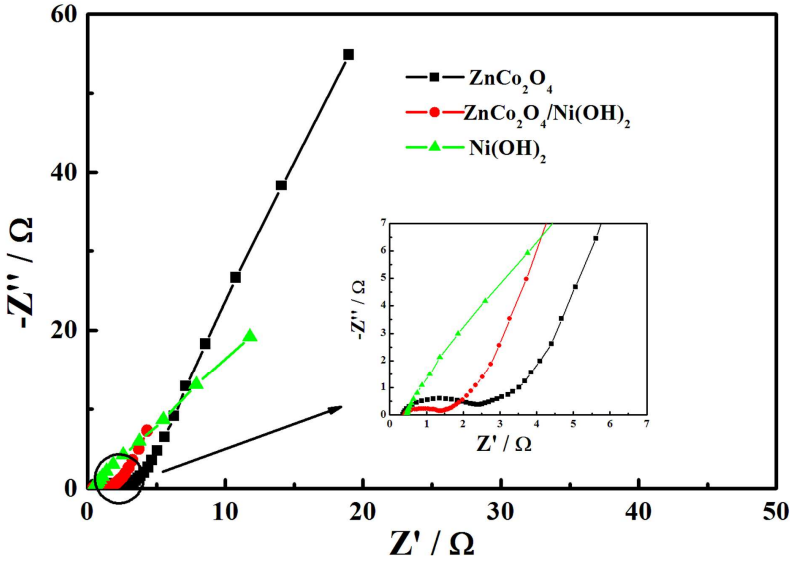

Figure 7 by H. X. Chuo, et al.

Rationally Designed Hierarchical $ZnCo_2O_4/Ni(OH)_2$ Composite Nanostructures for High-Performance Pseudocapacitor Electrodes

H. X. Chuo,[a] H. Gao, [a] Q. Yang, [a] N. Zhang, [b] W. B. Bu [a] and X. T. Zhang [*,a]

[a] *Key Laboratory for Photonic and Electronic Bandgap Materials, Ministry of Education，School of Physics and Electronic Engineering, Harbin Normal University, Harbin 150025, P. R. China.*

[b] *Department of Chemistry and Chemical Biology, Cornell University, Ithaca, USA.*

Graphical Abstract

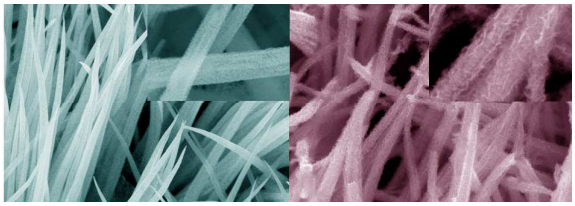

Hierarchical $ZnCo_2O_4/Ni(OH)_2$ nanostructures were rationally designed and successfully fabricated. They show excellent electrochemical performances.

* Corresponding author email: xtzhangzhang@hotmail.com